

# Enhancing Thermal Stability in Aminopyridine Iron(II)-Catalyzed Polymerization of Conjugated Dienes

Chuyang Jing, Liang Wang,\* Guangqian Zhu, Hongbin Hou, Li Zhou, and Qinggang Wang\*

Cite This: <https://dx.doi.org/10.1021/acs.organomet.0c00591>

Read Online

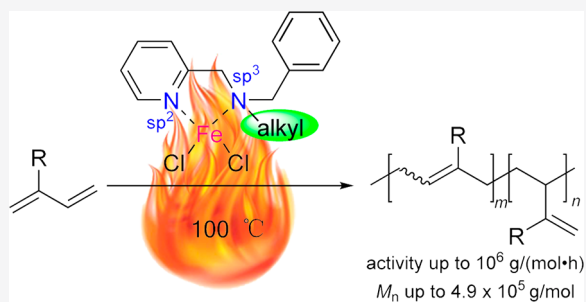
ACCESS |

Metrics & More

Article Recommendations

Supporting Information

**ABSTRACT:** A library of well-defined aminopyridine iron(II) precatalysts with a tertiary amine moiety have been prepared and serve as highly efficient precatalysts for polymerization of isoprene and other biobased conjugated dienes, delivering the corresponding polyolefin elastomers. These iron complexes were synthesized and further verified by ATR-IR, NMR, HR-MS spectroscopy, and elemental analysis. In addition, single-crystal diffraction analysis reveals that the structures of representative complexes **Fe-Me**, **Fe-Et**, and **Fe-*i*-Pr** all displayed chloride-bridged centrosymmetric binuclear geometry. Upon activation with MAO, the aminopyridine iron(II) complexes formed homogeneous Ziegler–Natta catalyst systems, which possessed excellent activities for the polymerization of isoprene. Interestingly, the activity of precatalysts increased as the steric hindrance was enhanced (**Fe-*i*-Pr** > **Fe-Bn** > **Fe-Et**), and the best activity was achieved by the **Fe-*i*-Pr** complex ( $2.34 \times 10^6 \text{ g}_{\text{polymer}} \text{ mol}^{-1} \text{ h}^{-1}$ ). In addition, the high activity that could almost be maintained even at 100 °C indicated that the **Fe-*i*-Pr** catalyst showed excellent thermal stability. The polymerizations of biobased myrcene and  $\beta$ -farnesene have been achieved smoothly by the **Fe-*i*-Pr** precatalyst, delivering high-molecular weight ( $\leq 4.9 \times 10^5 \text{ g/mol}$ ) “green rubber”.



## INTRODUCTION

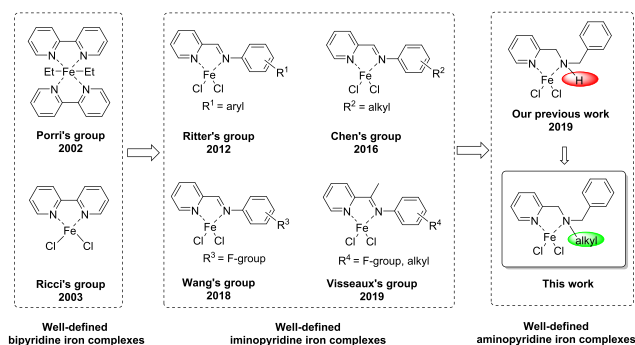
Polyolefin elastomers have wide applications and greatly enhance the convenience and quality of our modern life.<sup>1</sup> In particular, artificial polyisoprene, as one of the essential synthetic materials to replace natural rubber, has been widely applied in tires, tubes, and other industries.<sup>2</sup> Although significant studies of the highly efficient synthesis of various microstructure polyisoprene have been performed in both academia and industry during the past several decades, how to efficiently and precisely produce tailored microstructure polyisoprene is still a challenge for scientists.<sup>3</sup>

Recently, polyisoprenes with a side chain are more frequently utilized as important components in the high-performance manufacturing of tires, which results from their unique wet-skid resistance and low-rolling properties.<sup>4</sup> Meanwhile, side-chain olefins are beneficial for increasing the cross-link density of polyisoprenes.<sup>5</sup> Thus, the efficient synthetic approach of polyisoprenes with side chains by well-defined catalytic systems has attracted a great deal of attention. After economic and environmental issues of most coordinated catalytic systems have been taken into consideration, the well-defined iron-based catalysis gradually becomes one of the most attractive polymerization approaches with relatively high activity, low cost, and low toxicity.<sup>6</sup>

Throughout the process of 3,4-regularity-enriched polyisoprene in the field of iron catalysts, it could be found that the development of new material always benefits from the appearance of novel well-defined iron complexes. For the

framework of [N, N] bidentate ligands, researchers found that not only the ligand skeleton but also the hybridization of the nitrogen atom displayed significant effects on activity and selectivity of isoprene polymerization (Chart 1).<sup>7</sup> For example, a seminal report by Porri's group utilizes a symmetric

**Chart 1. Structural Evolution of Well-Defined [N, N] Bidentate Iron(II) Precatalysts for Isoprene Polymerization**

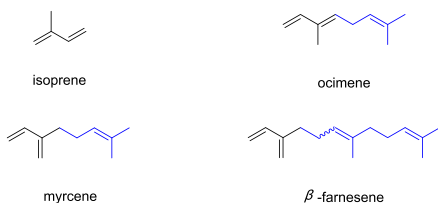


Received: September 7, 2020

bipyridine iron complex, to produce high 3,4-polyisoprene with high activities in 2002, in which the hybridized nitrogen atoms are all  $sp^2$ .<sup>8</sup> Later, Ritter, Chen, and other groups designed a novel iminopyridine iron complex, where the hybridized nitrogen atoms ( $sp^2$ ,  $sp^2$ ) are symmetric but ligand structures are unsymmetric, producing low to moderate 3,4-polyisoprene with high molecular weights.<sup>9</sup> Recently, new types of iron catalysts bearing aminopyridine ligands, for which both the geometric configuration and the hybridization of nitrogen atoms ( $sp^2$ ,  $sp^3$ ) are unsymmetric, were explored for isoprene polymerization by our group.<sup>10</sup> However, the reported aminopyridine iron catalysts showed moderate thermostability and the polyisoprenes with low  $M_n$  and wide  $D$ , which might be ascribed to the deprotonation of the catalyst by  $AlMe_3$  in MAO. In other words, multiple active species might exist in the polymerization system.

To maintain the precatalyst as a single-active species complex and improve its thermostability, we reported a series of novel tertiary aminopyridine iron(II) chloride catalysts by introducing an additional alkyl substituent on the amine moiety (Chart 1). A detailed study of their catalytic effects toward isoprene polymerization was performed. In addition to the isoprene derived from fossil sources, three biomonomers, myrcene, ocimene, and  $\beta$ -farnesene (Chart 2) obtained from turpentine,<sup>11</sup> were also investigated.

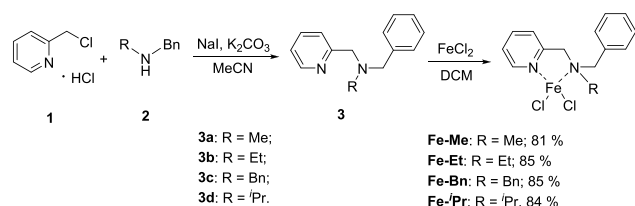
#### Chart 2. Monomer Structures



## RESULTS AND DISCUSSION

**Synthesis and Characterization of Aminopyridine Iron(II) Precatalysts.** These different aminopyridine ligands bearing methyl, ethyl, benzyl, and isopropyl groups on the amine segments have been prepared (Scheme 1). Compounds

#### Scheme 1. Preparation of Aminopyridine Iron(II) Precatalysts



3 were synthesized via nucleophilic reaction between 2-(chloromethyl)pyridine hydrochloride and  $N$ -alkylbenzylamine.<sup>12</sup> Next, at room temperature, equimolar amounts of ligand, anhydrous  $FeCl_2$ , and DCM were added sequentially to an anhydrous and oxygen-free reaction tube, and the heterogeneous solution was continuously stirred for 48 h. Finally, the target compound was obtained by filtration, concentration, and evaporation under vacuum. Further characterizations were mainly tested by HRMS-ESI, elemental analysis, ATR-IR, NMR, and single-crystal diffraction analysis.

Suitable crystals for X-ray diffraction analyses of iron complexes **Fe-Me**, **Fe-Et**, and **Fe- $i$ Pr** were grown from  $CH_2Cl_2$  saturation solutions at  $-30$  °C. The determined structures of **Fe-Me**, **Fe-Et**, and **Fe- $i$ Pr** all display chloride-bridged centrosymmetric binuclear geometry in Figures 1–3,

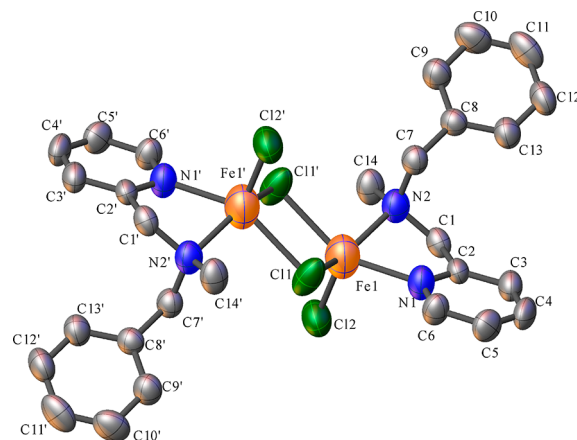


**Figure 1.** ORTEP drawing of the **Fe-Me** complex. Selected bond lengths (angstroms) and angles (degrees): Fe1–N1, 2.181(3); Fe1–N2, 2.232(3); Fe1–Cl1, 2.4569(12); Fe1–Cl2, 2.2799(12); Fe1–Cl1', 2.4511(11); N1–Fe1–N2, 77.32(8); N1–Fe1–Cl1', 147.36(9); N2–Fe1–Cl1, 146.63(9); Cl2–Fe1–Cl1, 111.79(5).

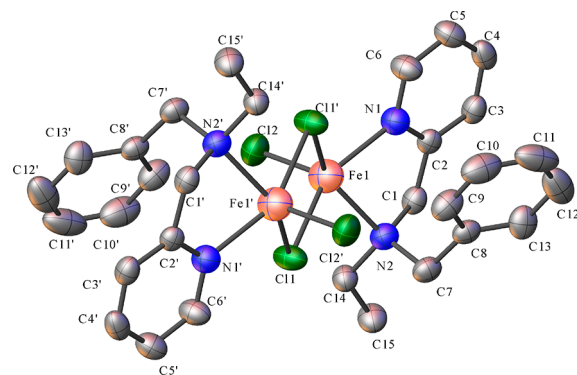


**Figure 2.** ORTEP drawing of the **Fe-Et** complex. Selected bond lengths (angstroms) and angles (degrees): Fe1–N1, 2.141(2); Fe1–N2, 2.253(3); Fe1–Cl1, 2.4667(9); Fe1–Cl2, 2.2840(10); Fe1–Cl1', 2.4477(9); N1–Fe1–N2, 77.08(9); N1–Fe1–Cl1, 150.23(7); N2–Fe1–Cl1', 146.16(7); Cl2–Fe1–Cl1, 108.21(4).

respectively. The geometric parameter  $\tau$  [ $\tau = (\beta - \alpha)/60^\circ$ ] values of **Fe-Me**, **Fe-Et**, and **Fe- $i$ Pr** utilized to judge the spatial configurations of the metal center as trigonal bipyramidal ( $\tau = 1$ ) or square pyramidal ( $\tau = 1$ ) are 0.01, 0.07, and 0.16, respectively.<sup>13</sup> It means that these dimeric structures adopted slightly distorted square pyramidal geometry, where N1<sub>pyridine</sub>, N2<sub>amino</sub>, Cl1'<sub>bridge</sub>, and Cl1<sub>bridge</sub> form the equatorial plane. The nonbridged chloride (Cl2) serves as the vertex. The iron center lies out of the plane by 0.657 Å (**Fe-Me**), 0.633 Å (**Fe-Et**), and 0.616 Å (**Fe- $i$ Pr**). Due to donor atom N2 and bridging atom C1 having  $sp^3$  hybridization, the five-membered chelate N–C–C–N–Fe rings are significantly distorted, generating two twisty planes with angles of 51.45° (**Fe-Me**), 38.82° (**Fe-Et**), and 40.17° (**Fe- $i$ Pr**) between the Fe1–N2–N1 and N2–C1–C2 planes.

The N1–Fe1–N2 bond angles of **Fe-Me**, **Fe-Et**, and **Fe- $i$ Pr** are comparable (77.32°, 77.08°, and 76.27°, respectively) but

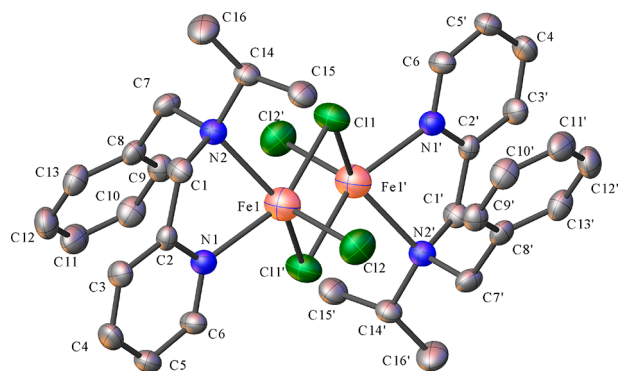


**Figure 3.** ORTEP drawing of the Fe-*i*-Pr complex. Selected bond lengths (angstroms) and angles (degrees): Fe1–N1, 2.149(3); Fe1–N2, 2.324(3); Fe1–Cl1, 2.4331(12); Fe1–Cl2, 2.3107(12); Fe1–Cl1', 2.5022(12); N1–Fe1–N2, 76.27(12); N1–Fe1–Cl1, 154.01(9); N2–Fe1–Cl1', 144.51(9); Cl2–Fe1–Cl1, 108.04(4).

slightly decreased as the steric hindrance of alkyl groups increased. In comparison with the planar chelate N–C–N–Fe ring and N1–Fe1–N2 bite angles for iminopyridine iron complexes, the steric hindrance of the metal center becomes crowded when the iminopyridine ligand is transferred to the aminopyridine ligand. Gao's group had reported a similar conclusion when the  $\alpha$ -diamine palladium complex was reduced to the  $\alpha$ -diamine palladium complex.<sup>14</sup>

The Fe–N<sub>amine</sub> bond lengths of 2.232(3) Å in Fe-Me, 2.253(3) Å in Fe-Et, and 2.324(3) Å in Fe-*i*-Pr are longer than the Fe–N<sub>imine</sub> bond length in analogous iminopyridine iron(II) complexes [2.121(6) Å in Ritter's complex<sup>9a</sup> and 2.197(7) Å in Wang's complex<sup>15</sup>], which indicates that the coordination ability of the sp<sup>2</sup> N atom is better than that of the sp<sup>3</sup> N atom in this work. In other words, the Lewis acidity of the aminopyridine-ligated iron center is stronger than that of the iminopyridine-ligated iron center. These results further confirmed that the electrophilic ability of the iron center in the iminopyridine motif is weaker than that of the aminopyridine motif, which was reported by our previous work.

**Polymerization of Isoprene.** The catalytic performances of isoprene polymerization catalyzed by tertiary amino-pyridine-iron(II) precursors have been investigated, and the resulting data are summarized in Table 1. Initially, different iron(II) complexes were studied upon activation with MAO in 2 h. The lowest activity was observed in the Fe-Et complex, which was substituted with ethyl. Interestingly, the catalytic activities gradually increased with a group that was relatively bulkier than the ethyl group. The Fe-*i*-Pr complex exhibited the highest activity of  $6.8 \times 10^4$  g<sub>polymer</sub> mol<sup>-1</sup> h<sup>-1</sup>, which has the most sterically hindered group (Table 1, entry 5). It was notable that the reaction catalyzed by Fe-*i*-Pr was still full conversion ( $8.16 \times 10^5$  g<sub>polymer</sub> mol<sup>-1</sup> h<sup>-1</sup>) even if the polymerization time decreased to 10 min (Table 1, entry 6). In general, the catalytic activity is significantly dependent on the steric effect of the ligand and the Lewis acidity of the iron center. Additionally, increasing the steric hindrance of the ligand inhibits the coordination of the monomer with the metal center, leading to a decrease in the catalyst activity. However, it was observed that the degree of spatial opening around the iron center changes inconspicuously when the alkyl group on the amine is replaced with ethyl to isopropyl according to similar N1–Fe1–N2 bite angles ( $77.08^\circ$  and  $76.27^\circ$  for Fe-Et and Fe-*i*-Pr, respectively). Meanwhile, the Fe–N<sub>amine</sub> and Fe–N<sub>pyridine</sub> bond lengths in Fe-Et are all shorter than those in Fe-*i*-Pr. This demonstrated that the iron center of Fe-*i*-Pr shows Lewis acidity that is stronger than that of Fe-Et, thus facilitating the coordination and insertion of isoprene and leading to a higher activity.

In addition, the molecular weight of polyisoprenes was highly dependent on the steric hindrance of the catalyst, in which the molecular weight is decreased with the steric hindrance increased, and all of the  $M_n$  values fall in the range of  $2.7$ – $4.3 \times 10^5$  g/mol (Figure 4). It could be associated with a bulkier ligand having a strong steric repulsion effect with polymer chains, thus facilitating the transfer of the polymer chain from iron active species to aluminum. In addition, a relatively narrow and monomodal molecular weight distribution (1.8–2.0) was characteristic of the resultant polymer,

**Table 1.** Fe Complexes Catalyzed Isoprene Polymerizations under Different Conditions<sup>a</sup>

entry	catalyst	time (min)	<i>T</i> (°C)	yield (%)	activity <sup>g</sup>	microstructure <sup>h</sup> (%)			$M_n^i$ ( $\times 10^{-5}$ )	$D^i$
						<i>cis</i> -1,4	3,4	<i>trans</i> -1,4		
1	Fe-Me	120	25	>99	6.8	37	63	–	4.3	1.8
2	Fe-Me	10	25	81	66.0	39	61	–	4.4	1.9
3	Fe-Et	120	25	55	3.7	40	60	–	3.6	1.8
4	Fe-Bn	120	25	77	5.3	42	58	–	3.1	2.0
5	Fe- <i>i</i> -Pr	120	25	>99	6.8	44	56	–	2.7	2.0
6	Fe- <i>i</i> -Pr	10	25	>99	81.6	45	55	–	3.0	1.9
7	Fe- <i>i</i> -Pr	10	50	>99	81.6	40	49	11	2.7	1.9
8	Fe- <i>i</i> -Pr	10	70	>99	81.6	41	50	9	1.4	2.0
9	Fe- <i>i</i> -Pr	10	90	91	74.4	40	47	13	1.6	1.8
10	Fe- <i>i</i> -Pr	10	100	90	73.2	40	47	13	1.5	2.0
11 <sup>b</sup>	Fe- <i>i</i> -Pr	10	25	58	234.0	45	55	–	3.8	1.9
12 <sup>c</sup>	Fe- <i>i</i> -Pr	10	25	96	78.0	42	53	5	2.5	2.0
13 <sup>d</sup>	Fe- <i>i</i> -Pr	10	25	92	75.0	42	52	6	4.0	1.9
14 <sup>e</sup>	Fe- <i>i</i> -Pr	10	25	>99	81.6	47	53	–	2.9	2.0
15 <sup>f</sup>	Fe- <i>i</i> -Pr	10	25	>99	81.6	47	53	–	2.4	2.0

<sup>a</sup>Polymerization conditions: 5 mL of toluene, 10  $\mu$ mol of an iron catalyst, 20 mmol of isoprene, 25 °C, MAO as a co-catalyst (5 mmol). <sup>b</sup>Toluene (25 mL) as the solvent; IP/Fe ratio of 10000. <sup>c</sup>MAO/Fe ratio of 300. <sup>d</sup>MAO/Fe ratio of 200. <sup>e</sup>DMAO/Fe ratio of 500. <sup>f</sup>MMAO/Fe ratio of 500. <sup>g</sup>At  $10^4$  g<sub>polymer</sub> mol<sup>-1</sup> h<sup>-1</sup>. <sup>h</sup>Determined by <sup>1</sup>H and <sup>13</sup>C NMR. <sup>i</sup>Determined by gel permeation chromatography (GPC).

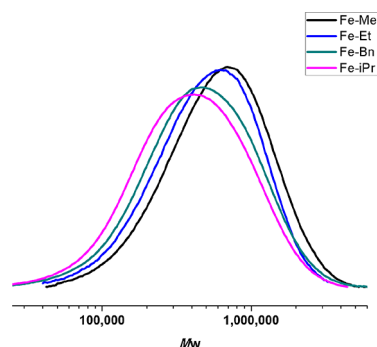


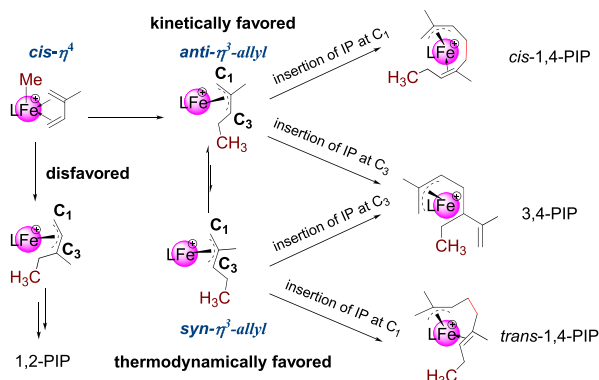
**Figure 4.** GPC curves of the polymer obtained from the title catalysts (Table 1, entries 1 and 3–5).

suggesting that the true active species is a single-site center during the polymerization. This result is impressive in comparison with the previously reported secondary 2-[*N,N*-(H)(benzyl)aminomethyl]pyridine iron(II) complex system, which probably included multiple active species and generated low-molecular weight polymers ( $3.9 \times 10^4$  g/mol) with a wide molecular weight distribution of 3.9.

The stereoselectivity and regioselectivity of the obtained polymers have been analyzed by  $^1\text{H}$  and  $^{13}\text{C}$  nuclear magnetic resonance and established by characteristic peaks in the literature.<sup>16</sup> As a whole, all of the polymers possessed slightly different amounts of *cis*-1,4-regularity and 3,4-regularity, and those without *trans*-1,4-regularity were generated at ambient temperature (Table 1 and Figure S32). For instance, the polyisoprene obtained from the Fe-Me complex, bearing the least sterically hindered group, exhibited 37% *cis*-1,4-regularity and 63% 3,4-regularity, while the polymer obtained from the Fe-*i*Pr complex exhibited 44% *cis*-1,4-regularity and 56% 3,4-regularity. In comparison, the 1,4-regularity of the polymer obtained from the iminopyridine iron catalysts was higher than that of aminopyridine iron(II) complexes in this work.<sup>9,15</sup>

The foregoing X-ray diffraction analysis has found that the Lewis acidity of the aminopyridine-ligated iron center is stronger than that of the iminopyridine-ligated iron center. Thus, the electrophilic aminopyridine iron center ( $\text{LFe}^{2+}$ ) tends to coordinate with the incoming monomer through *cis*- $\eta^4$  mode rather than  $\eta^2$  mode (Scheme 2).<sup>6j,10</sup> In addition, the 1,4-regularity is generated via the active iron center bound to the C1 position of *anti*- $\eta^3$  or *syn*- $\eta^3$  allyl intermediates, while

**Scheme 2. Possible Selectivity Approach for the Polymerization of Isoprene Catalyzed by Cationic [(Aminopyridine)FeMe]<sup>2+</sup>**



3,4-regularity is achieved though the active iron center bound to the C3 position.<sup>17</sup> When the iron center is bound to the C1 position via *syn*- $\eta^3$  allyl intermediates, isomerized by the *anti*- $\eta^3$ -allyl intermediates, the *trans*-1,4-regularity would become visible. However, this approach is uncompetitive in terms of energy.<sup>18</sup> As shown in Table 1 in the microstructure of the resultant polymer generated from different catalysts in this research, the change in selectivity affected by the steric hindrance of those amino pyridine catalysts is not conspicuous. It can be explained by comparable N1–Fe1–N2 bite angles ( $77.32^\circ$ ,  $77.08^\circ$ , and  $76.27^\circ$  for Fe-Me, Fe-Et, and Fe-*i*Pr, respectively) in single-crystal X-ray structures. We observed that the degree of spatial opening around the iron center changes inconspicuously when the alkyl group on the amine is replaced.

The Fe-*i*Pr precatalyst was selected to evaluate the influence of other conditions, such as the type and quantity of the cocatalyst, IP/Fe ratios, and reaction temperatures. The temperature is critical for polymerization; thus, reaction temperatures were improved first from 25 to 100 °C (Table 1, entries 6–10). According to the data, full conversion was still achieved within 10 min when the temperature was 50 or 70 °C. Remarkably, even if the reaction temperature was improved to 100 °C, the yields only slightly decreased to 90%. This result reflected the fact that the active iron species of the Fe-*i*Pr complex possess excellent thermal stability during the course of the polymerization. It was a remarkable improvement compared to previous results. For example, the yield of polyisoprene catalyzed by the secondary aminopyridine iron(II) chloride complex decreased from 100% to 71% as the temperature increased from 25 to 50 °C,<sup>10</sup> and the yield of polyisoprene obtained from the terpyridine/FeCl<sub>2</sub> complex was observed to decrease sharply from 99% to 24% when the temperature was increased from 25 to 60 °C.<sup>7a</sup> These results may be ascribed to the unstable state of the active species at high temperatures.<sup>19</sup> Therefore, the Fe-*i*Pr complex has excellent thermal tolerance, which probably resulted from the protection of the bulky substituent of the amine moiety. Similarly, considerable thermal stable complexes that introduced bulky groups have been reported during the polymerization of olefin, such as bulky steric  $\alpha$ -diimine nickel/palladium catalysts<sup>20</sup> and bis(imino)pyridine iron/cobalt catalysts.<sup>21</sup>

To the best of our knowledge, this iron complex has the best thermal stability in isoprene polymerization. Expectedly, the molecular weights of polymers decreased when the reaction temperature was increased. It might be attributed to the increased rate of chain propagation being lower than the rate of the transfer and termination reaction when the temperature was enhanced.<sup>22</sup> With regard to the stereoselectivity and regioselectivity of the obtained polymer prepared under higher-temperature conditions, it could be found that a higher temperature had a weak influence on the regioselectivity of monomer insertion, while 9–13% *trans*-1,4-selectivity appeared at different high temperatures (Figure 5). This result could be explained by *anti*-*syn* isomerization through  $\pi$ - $\sigma$  rearrangement.<sup>18,19,23</sup> At high temperatures, the *anti* (kinetic) active species conformer gradually transformed into the thermodynamically stable *syn* isomer, increasing the quantity of *trans*-1,4-regularity of the corresponding polyisoprene.

In addition, when the IP/Fe ratio was increased to 10000, although the conversion of monomer was reduced, the activity was improved to  $2.34 \times 10^6$  g<sub>polymer</sub> mol<sup>-1</sup> h<sup>-1</sup> within 10 min

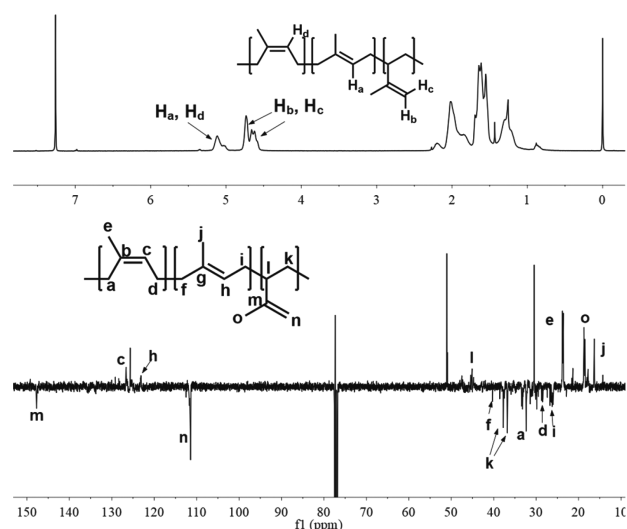


**Figure 5.**  $^1\text{H}$  and DEPT-Q NMR spectra of polyisoprene (Table 1, entry 10) obtained with  $\text{Fe}^i\text{-Pr}$  and MAO at  $100\text{ }^\circ\text{C}$ .

(Table 1, entry 11), which indicated that the capacity of  $\text{Fe}^i\text{-Pr}$ -catalyzed isoprene polymerization was superior to that of secondary aminopyridine iron(II) complexes with a maximum value of  $1.9 \times 10^6 \text{ g}_{\text{polymer}} \text{ mol}^{-1} \text{ h}^{-1}$  previously reported.<sup>10</sup> Next, the Al/Fe ratio was investigated (Table 1, entries 12 and 13). It was noted that the activity and selectivity were nearly invariant as the Al/Fe ratio decreased from 500 to 200. Furthermore, different types of co-catalysts were subsequently tested. It could be found that when MMAO or DMAO was utilized as a co-catalyst, no obvious differences have been observed in terms of selectivity, activity, and molecular weight.

**Polymerization of Biodienes.** At present, due to the unsustainable renewable nature of petroleum resources and the energy crisis, it is greatly important to search for biobased monomers to replace petroleum-based monomers, to prepare biobased green rubber materials, and to alleviate the current severe energy crisis and environmental problems. Thus, the highest-catalytic activity  $\text{Fe}^i\text{-Pr}$  iron(II) complex has also been investigated with respect to polymerizations of several biodienes, such as ocimene, myrcene, and  $\beta$ -farnesene (Table 2). As shown in Table 2, the  $\text{Fe}^i\text{-Pr}$  complex cannot promote ocimene polymerization but exhibits outstanding performance in the polymerization of myrcene with an activity of  $6.0 \times 10^4$

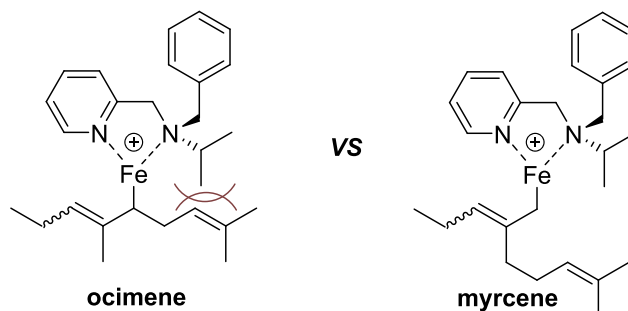
**Table 2.** Polymerization of Several Biomass Monomers Using  $\text{Fe}^i\text{-Pr}$  and MAO<sup>a</sup>

entry	monomer	yield (%)	activity <sup>c</sup>	microstructure <sup>d</sup> (%)		$M_n^e$ ( $\times 10^{-5}$ )	$\bar{D}^e$
				1,4	3,4		
1	ocimene	0	0	—	—	—	—
2	myrcene	89	6.0	59	41	3.1	1.9
3	$\beta$ -farnesene	>99	10.2	68	32	3.4	1.9
4 <sup>b</sup>	$\beta$ -farnesene	68	13.7	75	25	4.9	1.9

<sup>a</sup>Conditions: solvent consisting of 5 mL of toluene, 10  $\mu\text{mol}$  of  $\text{Fe}^i\text{-Pr}$  as the catalyst, and 10 mmol of monomer,  $25\text{ }^\circ\text{C}$ , MAO as the co-catalyst (5 mmol), 2 h. <sup>b</sup>With 20 mmol of  $\beta$ -farnesene. <sup>c</sup>At  $10^4 \text{ g}_{\text{polymer}} \text{ mol}^{-1} \text{ h}^{-1}$ . <sup>d</sup>Determined by  $^1\text{H}$  nuclear magnetic resonance. <sup>e</sup>Determined by gel permeation chromatography (GPC).

$\text{g}_{\text{polymer}} \text{ mol}^{-1} \text{ h}^{-1}$ . This indicated that the catalyst displayed excellent chemoselectivity and isomerselectivity. In other words, the polymerization approach could afford only poly- $\beta$ -isomers. It is expected that the long-chain group from ocimene covers more space around the metal center during the polymerization, leading to large steric hindrance between the monomer and active species (Chart 3). By contrast, the

**Chart 3.** Proposed Mechanistic Models for Coordination and Insertion of Ocimene and Myrcene



Potential steric hindrance of ocimene and myrcene

direction of the long-chain group from myrcene is away from the metal center. Hence, it is much easier for myrcene to coordinate or insert than ocimene during polymerization.

Furthermore, the  $\text{Fe}^i\text{-Pr}$  catalyst also showed appreciable catalytic potential with a maximum value of  $1.37 \times 10^5 \text{ g}_{\text{polymer}} \text{ mol}^{-1} \text{ h}^{-1}$  for polymerization of  $\beta$ -farnesene, which bears a tail that is longer than that of myrcene. With regard to the microstructure of the polymer, 1,4-selectivity microstructure (59%) is the dominant component of the polymyrcene catalyzed by  $\text{Fe}^i\text{-Pr}$ , while the poly- $\beta$ -farnesene is composed of a larger amount of 1,4-regularity (75%) and a smaller amount of 3,4-regularity (25%) (Figure 6). In comparison with

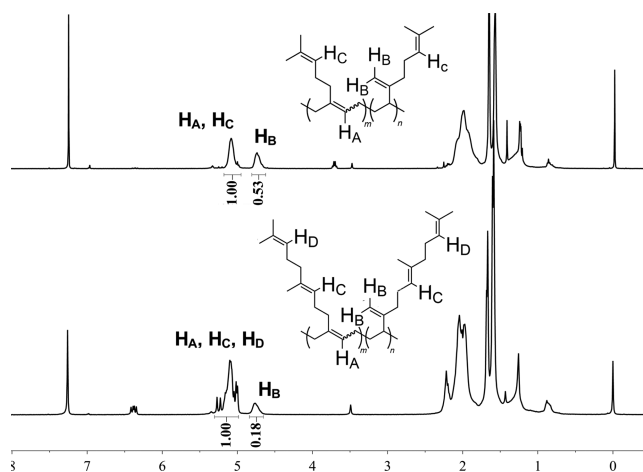


**Figure 6.**  $^1\text{H}$  NMR spectra of polymyrcene (Table 2, entry 2) and polyfarnesene (Table 2, entry 4) obtained with  $\text{Fe}^i\text{-Pr}$  and MAO.

polyisoprene, polymers catalyzed by the same  $\text{Fe}^i\text{-Pr}$  catalyst exhibited higher 1,4-regularity as the steric hindrance of the monomer increased, which indicated that the selectivity was highly dependent on the monomer. In the crowded environment around the iron center, the incoming monomers favor insertion at the active site of C1 rather than C3 (Scheme 2),

which suppresses the formation of 3,4-regularity resulting in a higher content of *cis*-1,4-regularity.<sup>19</sup> As for myrcene and  $\beta$ -farnesene polymerization, the longer tail of the monomer promoted the steric effects that control the regiochemistry of insertion.

## CONCLUSION

A library of well-defined aminopyridine iron(II) precatalysts were synthesized via the introduction of bulky alkyl groups instead of active hydrogen [N(H)]. The **Fe-Me**, **Fe-Et**, and **Fe-Pr** complexes showed a similar structure, which has chloride-bridged centrosymmetric binuclear geometry verified by single-crystal X-ray diffraction. These precatalysts showed excellent activities toward isoprene polymerization ( $\leq 2.34 \times 10^6$  g<sub>polymer</sub> mol<sup>-1</sup> h<sup>-1</sup>) upon activation by MAO, delivering polyconjugated dienes with high  $M_n$  values ( $1.5\text{--}4.4 \times 10^5$  g/mol) and a narrow  $\bar{D}$  range (1.8–2.0). More importantly, the **Fe-Pr** catalyst is a highly thermally stable bidentate iron(II) complex, which could efficiently promote the polymerization even at 100 °C. In addition, two renewable biodienes, myrcene and  $\beta$ -farnesene, were also efficiently polymerized by **Fe-Pr** to produce the poly- $\beta$ -isomer with high-molecular weight “green rubber”. Further insightful explorations of Fe-catalyzed polyolefin synthesis are under progress in our laboratory.

## EXPERIMENTAL SECTION

**General Procedure.** The standard Schlenk technique was used to deal with all water and oxygen sensitive reagents and complexes. All solvents and monomers need to be purified according to standards used previously. CDCl<sub>3</sub> was selected as a deuterated reagent, and the Bruker Avance III 400 MHz spectrometer was utilized to record NMR spectra. The Shanghai Institute of Organic Chemistry carried out an elemental analysis test under anhydrous and oxygen-free conditions on a Vario EL III elemental analyzer. Shanghai Jiao Tong University recorded mass spectra under anhydrous and oxygen-free conditions by maXis II of Bruker Daltonics Corp. and ACQUITYTM UPLC and Q-TOF MS Premier. The Bruker Smart diffractometer with a Mo  $K\alpha$  X-ray source was used to collect data at 298 K.  $M_n$  and  $\bar{D}$  values of polymers were collected at PL-GPC 220 of Agilent Technologies. DMAO was obtained by removing the solvent and residual trimethylaluminum of MAO. Other chemical materials were purchased without further purification before use.

**Synthesis of Ligands.** *N*-Benzyl-*N*-methyl-1-(pyridin-2-yl)methanamine (**3a**). At room temperature, the raw materials 2-(chloromethyl)pyridine hydrochloride (20 mmol, 1 equiv), sodium iodide (2.0 mmol, 0.1 equiv), and potassium carbonate (100 mmol, 5 equiv) were added in sequence in a 50 mL two-neck flask, and 50 mL of CH<sub>3</sub>CN was used as the solvent. After 5 min, the *N*-methylbenzylamine (50 mmol, 2.5 equiv) was added dropwise, and the solution was kept stirring for 12 h until thin layer chromatography showed that the reaction was over. Product **3a** was achieved as a yellow oil (3.63 g, 86% yield) purified by filtration, concentration, and silica gel column purification (1:1 PE:EtOAc). <sup>1</sup>H NMR (400 MHz, CDCl<sub>3</sub>, 298 K):  $\delta$  8.54 (d,  $J$  = 4.8 Hz, 1H), 7.64 (t,  $J$  = 7.6 Hz, 1H), 7.51 (d,  $J$  = 7.8 Hz, 1H), 7.37 (d,  $J$  = 7.6 Hz, 2H), 7.31 (t,  $J$  = 7.6 Hz, 2H), 7.24 (d,  $J$  = 7.2 Hz, 1H), 7.16–7.10 (m, 1H), 3.70 (s, 2H), 3.59 (s, 2H), 2.24 (s, 3H). <sup>13</sup>C NMR (100 MHz, CDCl<sub>3</sub>, 298 K):  $\delta$  159.79, 149.02, 139.04, 136.42, 128.98, 128.28, 127.04, 122.97, 121.94, 63.50, 62.15, 42.55. HRMS-ESI ( $m/z$ ): [M + H]<sup>+</sup> calcd for C<sub>14</sub>H<sub>17</sub>N<sub>2</sub>, 213.1392; found, 213.1392.

*N*-Benzyl-*N*-ethyl-1-(pyridin-2-yl)methanamine (**3b**). Product **3b** was achieved as a yellow oil (4.24 g, 94% yield) by an approach identical to that for the preparation of **3a** using *N*-ethylbenzylamine as the raw material (50.0 mmol, 2.5 equiv). <sup>1</sup>H NMR (400 MHz, CDCl<sub>3</sub>, 298 K):  $\delta$  8.49 (d,  $J$  = 4.8 Hz, 1H), 7.61 (td,  $J$  = 7.6, 1.8 Hz, 1H), 7.55 (dt,  $J$  = 7.8, 1.2 Hz, 1H), 7.41–7.34 (m, 2H), 7.34–7.25 (m, 2H), 7.27–7.16 (m, 1H), 7.09 (dd,  $J$  = 6.8, 4.8 Hz, 1H), 3.75 (s, 2H), 3.63

(s, 2H), 2.56 (q,  $J$  = 7.2 Hz, 2H), 1.08 (t,  $J$  = 7.2 Hz, 3H). <sup>13</sup>C NMR (100 MHz, CDCl<sub>3</sub>, 298 K):  $\delta$  160.65, 148.82, 139.66, 136.34, 128.79, 128.20, 126.84, 122.73, 121.75, 59.74, 58.13, 47.71, 12.01. HRMS-ESI ( $m/z$ ): [M + H]<sup>+</sup> calcd for C<sub>15</sub>H<sub>19</sub>N<sub>2</sub>, 227.1548; found, 227.1549.

*N,N*-Dibenzyl-1-(pyridin-2-yl)methanamine (**3c**). Product **3c** was produced as a yellow oil (1.21 g, 28% yield) by an approach identical to that for the preparation of **3a** by using 2-(chloromethyl)pyridine hydrochloride (15.0 mmol, 1 equiv), sodium iodide (2.0 mmol, 1.3 equiv), potassium carbonate (100.0 mmol, 6.6 equiv), and dibenzylamine (50.0 mmol, 3.3 equiv). <sup>1</sup>H NMR (400 MHz, CDCl<sub>3</sub>, 298 K):  $\delta$  8.49 (d,  $J$  = 4.8 Hz, 1H), 7.70–7.60 (m, 2H), 7.41 (d,  $J$  = 7.2 Hz, 4H), 7.32 (t,  $J$  = 7.4 Hz, 4H), 7.23 (s, 2H), 7.13 (t,  $J$  = 6.6 Hz, 1H), 3.74 (s, 2H), 3.62 (s, 4H). <sup>13</sup>C NMR (100 MHz, CDCl<sub>3</sub>, 298 K):  $\delta$  160.40, 148.91, 139.45, 136.59, 128.91, 128.41, 127.10, 122.85, 122.02, 59.94, 58.40. HRMS-ESI ( $m/z$ ): [M + H]<sup>+</sup> calcd for C<sub>20</sub>H<sub>21</sub>N<sub>2</sub>, 289.1705; found, 289.1695.

*N*-Benzyl-*N*-isopropyl-1-(pyridin-2-yl)methanamine (**3d**). Product **3d** was produced as a yellow oil (1.01 g, 30% yield) by an approach identical to that for the preparation of **3a** using *N*-isopropylbenzylamine as the raw material (22.5 mmol, 1.5 equiv). <sup>1</sup>H NMR (400 MHz, CDCl<sub>3</sub>, 298 K):  $\delta$  8.47 (d,  $J$  = 4.8 Hz, 1H), 7.62 (dd,  $J$  = 5.0, 1.6 Hz, 2H), 7.40 (d,  $J$  = 7.2 Hz, 2H), 7.29 (t,  $J$  = 7.4 Hz, 2H), 7.21 (t,  $J$  = 7.4 Hz, 1H), 7.11–7.06 (m, 1H), 3.77 (s, 2H), 3.64 (s, 2H), 2.96 (hept,  $J$  = 6.8 Hz, 1H), 1.10 (d,  $J$  = 6.6 Hz, 6H). <sup>13</sup>C NMR (100 MHz, CDCl<sub>3</sub>, 298 K):  $\delta$  161.65, 148.58, 140.61, 136.38, 128.53, 128.18, 126.69, 122.39, 121.62, 55.38, 53.97, 49.28, 17.81. HRMS-ESI ( $m/z$ ): [M + H]<sup>+</sup> calcd for C<sub>16</sub>H<sub>21</sub>N<sub>2</sub>, 241.1705; found, 241.1706.

**Synthesis of Ferrous Chloride Complexes.** *N*-Benzyl-*N*-methyl-1-(pyridin-2-yl)methanamine Ferrous Chloride (**Fe-Me**). Under anhydrous and oxygen-free conditions, anhydrous FeCl<sub>2</sub> (1.00 mmol, 1.0 equiv) and a dichloromethane (10 mL) solution of ligand **3a** (1.00 mmol, 1.0 equiv) were added in sequence to a 25 mL Schlenk tube, and the heterogeneous solution was kept stirring for 48 h at room temperature. Finally, the compound was obtained by filtration, concentration, washing with distilled hexane (2  $\times$  10 mL), and evaporation under vacuum. **Fe-Me** was afforded as a pale yellow powder (272.2 mg, 81% yield). ATR-IR (cm<sup>-1</sup>): 3098, 3012, 2924, 1605, 1508, 1455, 1444, 1213, 1156, 970, 850, 753, 703. <sup>1</sup>H NMR (400 MHz, CDCl<sub>3</sub>, 298 K):  $\delta$  124.5 ( $\Delta\nu_{1/2}$  = 1100 Hz), 105.9, 83.3, 73.1, 58.5 ( $\Delta\nu_{1/2}$  = 480 Hz), 52.0 ( $\Delta\nu_{1/2}$  = 450 Hz), 38.3 ( $\Delta\nu_{1/2}$  = 500 Hz), 7.9 ( $\Delta\nu_{1/2}$  = 150 Hz), -9.6 ( $\Delta\nu_{1/2}$  = 457 Hz). HRMS (ESI,  $m/z$ ): [M - FeCl<sub>2</sub>]<sup>+</sup> calcd for C<sub>28</sub>H<sub>32</sub>ClFeN<sub>4</sub>, 515.1665; found, 515.1666. Anal. Calcd for C<sub>14</sub>H<sub>16</sub>Cl<sub>2</sub>FeN<sub>2</sub>: C, 49.60; H, 4.76; N, 8.26. Found: C, 49.09; H, 4.88; N, 8.26.

*N*-Benzyl-*N*-ethyl-1-(pyridin-2-yl)methanamine Ferrous Chloride (**Fe-Et**). **Fe-Et** was afforded by an approach identical to that for the preparation of **Fe-Me** by using ligand **3b** as a yellow powder (302.3 mg, 85% yield). ATR-IR (cm<sup>-1</sup>): 3098, 2971, 2912, 1608, 1470, 1448, 1296, 1215, 1104, 1021, 993, 872, 752. <sup>1</sup>H NMR (400 MHz, CDCl<sub>3</sub>, 298 K):  $\delta$  165.6 ( $\Delta\nu_{1/2}$  = 450 Hz), 124.2 ( $\Delta\nu_{1/2}$  = 457 Hz), 89.7, 75.4, 59.5 ( $\Delta\nu_{1/2}$  = 387 Hz), 49.4 ( $\Delta\nu_{1/2}$  = 468 Hz), -1.7 ( $\Delta\nu_{1/2}$  = 230 Hz), -9.4 ( $\Delta\nu_{1/2}$  = 295 Hz), -33.4 ( $\Delta\nu_{1/2}$  = 750 Hz). HRMS (ESI,  $m/z$ ): [M - FeCl<sub>2</sub> + H]<sup>+</sup> calcd for C<sub>30</sub>H<sub>37</sub>Cl<sub>2</sub>FeN<sub>4</sub>, 579.1745; found, 579.1746. Anal. Calcd for C<sub>15</sub>H<sub>18</sub>Cl<sub>2</sub>FeN<sub>2</sub>: C, 51.03; H, 5.14; N, 7.93. Found: C, 50.99; H, 5.39; N, 7.83.

*N,N*-Dibenzyl-1-(pyridin-2-yl)methanamine Ferrous Chloride (**Fe-Bn**). **Fe-Bn** was afforded by an approach identical to that for the preparation of **Fe-Me** by using ligand **3c** as a yellow powder (176.0 mg, 85% yield). ATR-IR (cm<sup>-1</sup>): 3048, 3024, 2931, 1607, 1490, 1451, 1301, 1203, 1160, 1053, 965, 749. <sup>1</sup>H NMR (400 MHz, CDCl<sub>3</sub>, 298 K):  $\delta$  61.0 ( $\Delta\nu_{1/2}$  = 175 Hz), 53.9 ( $\Delta\nu_{1/2}$  = 153 Hz), 10.2 ( $\Delta\nu_{1/2}$  = 360 Hz), 7.5 ( $\Delta\nu_{1/2}$  = 67 Hz), -8.73 ( $\Delta\nu_{1/2}$  = 90 Hz). Anal. Calcd for C<sub>20</sub>H<sub>20</sub>Cl<sub>2</sub>FeN<sub>2</sub>: C, 57.86; H, 4.86; N, 6.75. Found: C, 57.70; H, 4.91; N, 6.94.

*N*-Benzyl-*N*-isopropyl-1-(pyridin-2-yl)methanamine Ferrous Chloride (**Fe-Pr**). **Fe-Pr** was afforded by an approach identical to that for the preparation of **Fe-Me** by using ligand **3d** as a yellow powder (310.0 mg, 84% yield). ATR-IR (cm<sup>-1</sup>): 3102, 2965, 2830, 1608, 1571, 1469, 1444, 1397, 1298, 1150, 1023, 845, 784. <sup>1</sup>H NMR

(400 MHz, CDCl<sub>3</sub>, 298 K):  $\delta$  152.2, 108.2, 82.3, 69.3 ( $\Delta\nu_{1/2}$  = 565 Hz), 65.0 ( $\Delta\nu_{1/2}$  = 925 Hz), 49.6 ( $\Delta\nu_{1/2}$  = 528 Hz), 13.5 ( $\Delta\nu_{1/2}$  = 518 Hz), 9.1 ( $\Delta\nu_{1/2}$  = 298 Hz), -10.2 ( $\Delta\nu_{1/2}$  = 216 Hz), -38.6. HRMS (ESI,  $m/z$ ): [M - FeCl + 2H]<sup>+</sup> calcd for C<sub>32</sub>H<sub>42</sub>Cl<sub>3</sub>FeN<sub>4</sub>, 643.1824; found, 643.1824. Anal. Calcd for C<sub>16</sub>H<sub>20</sub>Cl<sub>2</sub>FeN<sub>2</sub>: C, 52.35; H, 5.49; N, 7.63. Found: C, 51.43; H, 5.51; N, 7.27.

## ■ ASSOCIATED CONTENT

### Supporting Information

The Supporting Information is available free of charge at <https://pubs.acs.org/doi/10.1021/acs.organomet.0c00591>.

Determination of polybiobidene compositions, NMR spectra for ligands and polymers, GPC curves for polymers, and crystallographic data for Fe-Me, Fe-Et, and Fe-<sup>i</sup>Pr complexes (PDF)

### Accession Codes

CCDC 1970711, 1970714, and 1970716 contain the supplementary crystallographic data for this paper. These data can be obtained free of charge via [www.ccdc.cam.ac.uk/data\\_request/cif](http://www.ccdc.cam.ac.uk/data_request/cif), or by emailing [data\\_request@ccdc.cam.ac.uk](mailto:data_request@ccdc.cam.ac.uk), or by contacting The Cambridge Crystallographic Data Centre, 12 Union Road, Cambridge CB2 1EZ, UK; fax: +44 1223 336033.

## ■ AUTHOR INFORMATION

### Corresponding Authors

Liang Wang – Key Laboratory of Biobased Materials, Qingdao Institute of Bioenergy and Bioprocess Technology, Chinese Academy of Sciences, Qingdao 266101, China; Email: [wangliang@qibebt.ac.cn](mailto:wangliang@qibebt.ac.cn)

Qinggang Wang – Key Laboratory of Biobased Materials, Qingdao Institute of Bioenergy and Bioprocess Technology, Chinese Academy of Sciences, Qingdao 266101, China; [orcid.org/0000-0003-1851-7078](https://orcid.org/0000-0003-1851-7078); Email: [wangqg@qibebt.ac.cn](mailto:wangqg@qibebt.ac.cn)

### Authors

Chuyang Jing – Key Laboratory of Biobased Materials, Qingdao Institute of Bioenergy and Bioprocess Technology, Chinese Academy of Sciences, Qingdao 266101, China

Guangqian Zhu – Key Laboratory of Biobased Materials, Qingdao Institute of Bioenergy and Bioprocess Technology, Chinese Academy of Sciences, Qingdao 266101, China; Center of Materials Science and Optoelectronics Engineering, University of Chinese Academy of Sciences, Beijing 100049, China

Hongbin Hou – Key Laboratory of Biobased Materials, Qingdao Institute of Bioenergy and Bioprocess Technology, Chinese Academy of Sciences, Qingdao 266101, China

Li Zhou – Key Laboratory of Biobased Materials, Qingdao Institute of Bioenergy and Bioprocess Technology, Chinese Academy of Sciences, Qingdao 266101, China

Complete contact information is available at:

<https://pubs.acs.org/doi/10.1021/acs.organomet.0c00591>

### Notes

The authors declare no competing financial interest.

## ■ ACKNOWLEDGMENTS

Generous support by the Major Science and Technology Innovation Program of Shandong Province (2018CXGC1105), the Young Taishan Scholars Program of

Shandong Province (tsqn201812112), “135” Projects Fund of the CAS-QIBEBT Director Innovation Foundation, and the DICP& QIBEBT United Foundation (UN201701) is gratefully acknowledged.

## ■ REFERENCES

- (1) (a) Nakamura, A.; Ito, S.; Nozaki, K. Coordination-Insertion Copolymerization of Fundamental Polar Monomers. *Chem. Rev.* **2009**, *109*, 5215–5244. (b) Li, G.; Lamberti, M.; Roviello, G.; Pellecchia, C. New Titanium and Hafnium Complexes Bearing [–NNN–] Pyrrolylpyridylamido Ligands as Olefin Polymerization Catalysts. *Organometallics* **2012**, *31*, 6772–6778. (c) Chen, Z.; Li, J.-F.; Tao, W.-J.; Sun, X.-L.; Yang, X.-H.; Tang, Y. Copolymerization of Ethylene with Functionalized Olefins by [ONX] Titanium Complexes. *Macromolecules* **2013**, *46*, 2870–2875. (d) Weberski, M. P., Jr.; Chen, C.; Delferro, M.; Marks, T. J. Ligand Steric and Fluoroalkyl Substituent Effects on Enchainment Cooperativity and Stability in Bimetallic Nickel(II) Polymerization Catalysts. *Chem. - Eur. J.* **2012**, *18*, 10715–10732. (e) Zhang, D.; Chen, C. Influence of Polyethylene Glycol Unit on Palladium- and Nickel-Catalyzed Ethylene Polymerization and Copolymerization. *Angew. Chem., Int. Ed.* **2017**, *56*, 14672–14676. (f) Wang, Z.; Liu, Q.; Solan, G. A.; Sun, W.-H. Recent Advances in Ni-mediated Ethylene Chain Growth: N-imine-donor Ligand Effects on Catalytic Activity, Thermal Stability and Oligo/polymer Structure. *Coord. Chem. Rev.* **2017**, *350*, 68–83. (g) Chen, M.; Chen, C. A Versatile Ligand Platform for Palladium- and Nickel-Catalyzed Ethylene Copolymerization with Polar Monomers. *Angew. Chem., Int. Ed.* **2018**, *57*, 3094–3098. (h) Muhammad, Q.; Tan, C.; Chen, C. Concerted steric and electronic effects on alpha-diimine nickel- and palladium-catalyzed ethylene polymerization and copolymerization. *Sci. Bull.* **2020**, *65*, 300–307. (i) Tan, C.; Pang, W. M.; Chen, C. A Phenol-containing alpha-Diimine Ligand for Nickel- and Palladium-Catalyzed Ethylene Polymerization. *Chin. J. Polym. Sci.* **2019**, *37*, 974–980. (j) Zhou, S.; Chen, C. Synthesis of silicon-functionalized polyolefins by subsequent cobalt-catalyzed dehydrogenative silylation and nickel-catalyzed copolymerization. *Sci. Bull.* **2018**, *63*, 441–445. (k) Wang, F.; Tian, S.; Li, R.; Li, W.; Chen, C. Ligand steric effects on naphthyl-alpha-diimine nickel catalyzed alpha-olefin polymerization. *Chin. J. Polym. Sci.* **2018**, *36*, 157–162.
- (2) (a) Wang, X.; Fan, L.; Huang, C.; Liang, T.; Guo, C.-Y.; Sun, W.-H. Highly cis-1,4 Selective Polymerization of Isoprene Promoted by alpha-diimine Cobalt(II) Chlorides. *J. Polym. Sci., Part A: Polym. Chem.* **2016**, *54*, 3609–3615. (b) Li, S.; Cui, D.; Li, D.; Hou, Z. Highly 3,4-Selective Polymerization of Isoprene with NPN Ligand Stabilized Rare-Earth Metal Bis(alkyl)s. Structures and Performances. *Organometallics* **2009**, *28*, 4814–4822. (c) Liu, B.; Sun, G.; Li, S.; Liu, D.; Cui, D. Isoprene Polymerization with Iminophosphonamide Rare-Earth-Metal Alkyl Complexes: Influence of Metal Size on the Regio- and Stereoselectivity. *Organometallics* **2015**, *34*, 4063–4068.
- (3) (a) Ricci, G.; Sommazzi, A.; Masi, F.; Ricci, M.; Boglia, A.; Leone, G. Well-defined Transition Metal Complexes with Phosphorus and Nitrogen Ligands for 1,3-dienes Polymerization. *Coord. Chem. Rev.* **2010**, *254*, 661–676. (b) Zhang, Z.; Cui, D.; Wang, B.; Liu, B.; Yang, Y. *Molecular Catalysis of Rare-earth Elements*; Springer: Berlin, 2010; pp 49–108. (c) Hu, Y.; Yu, Q.; Jiang, L.; Zhang, X. Iron-based Catalysts for Conjugated Diene Polymerization and the Polymer Properties. *Kexue Tongbao* **2016**, *61*, 3315–3325.
- (4) (a) Yoshioka, A.; Komuro, K.; Ueda, A.; Watanabe, H.; Akita, S.; Masuda, T.; Nakajima, A. Structure and Physical Properties of High-vinyl Polybutadiene Rubbers and their Blends. *Pure Appl. Chem.* **1986**, *58*, 1697–1706. (b) Wolpers, J.; Fuchs, H. B.; Herrmann, C.; Hellermann, W.; Nordsiek, K. H.; Fuchs, H.; Nordsiek, K. 3,4-Polyisoprene-Containing Rubber Blend Mixtures for Tire Treads. US5104941-A, 1992.
- (5) Liu, Y.; Lu, A.; Deng, Z.; Shi, D.; Li, J. Effect of Vinyl Concentration on the Characteristics of Silicone Rubber Vulcanization. *J. Funct. Mater.* **2013**, *44*, 488–492.

- (6) (a) Dawans, F.; Teyssie, P. Equimolecular Binary Polydienes II. Cobalt Catalysts for the Preparation of Equibinary Polyisoprenes. *Makromol. Chem.* **1967**, *109*, 68–80. (b) Ricci, G.; Battistella, M.; Porri, L. Chemoselectivity and Stereospecificity of Chromium(II) Catalysts for 1,3-Diene Polymerization. *Macromolecules* **2001**, *34*, 5766–5769. (c) Yao, C.; Liu, D.; Li, P.; Wu, C.; Li, S.; Liu, B.; Cui, D. Highly 3,4-Selective Living Polymerization of Isoprene and Copolymerization with  $\epsilon$ -Caprolactone by an Amidino N-Heterocyclic Carbene Ligated Lutetium Bis(alkyl) Complex. *Organometallics* **2014**, *33*, 684–691. (d) Wang, B.; Cui, D.; Lv, K. Highly 3,4-Selective Living Polymerization of Isoprene with Rare Earth Metal Fluorenyl N-Heterocyclic Carbene Precursors. *Macromolecules* **2008**, *41*, 1983–1988. (e) Zhang, L.; Nishiura, M.; Yuki, M.; Luo, Y.; Hou, Z. Isoprene Polymerization with Yttrium Amidinate Catalysts: Switching the Regio- and Stereoselectivity by Addition of AlMe<sub>3</sub>. *Angew. Chem., Int. Ed.* **2008**, *47*, 2642–2645. (f) Li, X.; Nishiura, M.; Hu, L.; Mori, K.; Hou, Z. Alternating and Random Copolymerization of Isoprene and Ethylene Catalyzed by Cationic Half-Sandwich Scandium Alkyls. *J. Am. Chem. Soc.* **2009**, *131*, 13870–13882. (g) Chen, J.; Gao, Y.; Xiong, S.; Delferro, M.; Lohr, T. L.; Marks, T. J. Metal and Counteranion Nuclearity Effects in Organoscandium-Catalyzed Isoprene Polymerization and Copolymerization. *ACS Catal.* **2017**, *7*, 5214–5219. (h) Fürstner, A. Iron Catalysis in Organic Synthesis: A Critical Assessment of What It Takes To Make This Base Metal a Multitasking Champion. *ACS Cent. Sci.* **2016**, *2*, 778–789. (i) Liu, B.; Li, L.; Sun, G.; Liu, J.; Wang, M.; Li, S.; Cui, D. 3,4-Polymerization of Isoprene by Using NSN- and NPN-Ligated Rare Earth Metal Precursors: Switching of Stereo Selectivity and Mechanism. *Macromolecules* **2014**, *47*, 4971–4978. (j) Champouret, Y.; Hashmi, O. H.; Visseaux, M. Discrete Iron-based Complexes: Applications in Homogeneous Coordination-insertion Polymerization Catalysis. *Coord. Chem. Rev.* **2019**, *390*, 127–170.
- (7) (a) Nakayama, Y.; Baba, Y.; Yasuda, H.; Kawakita, K.; Ueyama, N. Stereospecific Polymerizations of Conjugated Dienes by Single Site Iron Complexes Having Chelating N,N,N-Donor Ligands. *Macromolecules* **2003**, *36*, 7953–7958. (b) Zhang, X.; Zhu, G.; Mahmood, Q.; Zhao, M.; Wang, L.; Jing, C.; Wang, X.; Wang, Q. Iminoimidazole Based Co(II) and Fe(II) Complexes: Syntheses, Characterization, and Catalytic Behaviors for Isoprene Polymerization. *J. Polym. Sci., Part A: Polym. Chem.* **2019**, *57*, 767–775.
- (8) Bazzini, C.; Giarrusso, A.; Porri, L. Diethylbis(2,29-bipyridine)-iron/MAO. A Very Active and Stereospecific Catalyst for 1,3-Diene Polymerization. *Macromol. Rapid Commun.* **2002**, *23*, 922.
- (9) (a) Raynaud, J.; Wu, J. Y.; Ritter, T. Iron-catalyzed Polymerization of Isoprene and other 1,3-dienes. *Angew. Chem., Int. Ed.* **2012**, *51*, 11805–11808. (b) Guo, L.; Jing, X.; Xiong, S.; Liu, W.; Liu, Y.; Liu, Z.; Chen, C. Influences of Alkyl and Aryl Substituents on Iminopyridine Fe(II)- and Co(II)-Catalyzed Isoprene Polymerization. *Polymers* **2016**, *8*, 389–400. (c) Zhu, G.; Zhang, X.; Zhao, M.; Wang, L.; Jing, C.; Wang, P.; Wang, X.; Wang, Q. Influences of Fluorine Substituents on Iminopyridine Fe(II)- and Co(II)-Catalyzed Isoprene Polymerization. *Polymers* **2018**, *10*, 934–948. (d) Hashmi, O. H.; Champouret, Y.; Visseaux, M. Highly Active Iminopyridyl Iron-Based Catalysts for the Polymerization of Isoprene. *Molecules* **2019**, *24*, 3024–3020.
- (10) Jing, C.; Wang, L.; Mahmood, Q.; Zhao, M.; Zhu, G.; Zhang, X.; Wang, X.; Wang, Q. Synthesis and Characterization of Aminopyridine Iron(II) Chloride Catalysts for Isoprene Polymerization: Sterically Controlled Monomer Enchainment. *Dalton Trans.* **2019**, *48*, 7862–7874.
- (11) (a) Liu, B.; Liu, D.; Li, S.; Sun, G.; Cui, D. High Trans-1,4 (co)polymerization of  $\beta$ -myrcene and Isoprene with an Iminophosphonamide Lanthanum Catalyst. *Chin. J. Polym. Sci.* **2016**, *34*, 104–110. (b) Naddeo, M.; Buonerba, A.; Luciano, E.; Grassi, A.; Proto, A.; Capacchione, C. Stereoselective Polymerization of Biosourced Terpenes  $\beta$ -myrcene and  $\beta$ -ocimene and their Copolymerization with Styrene Promoted by Titanium Catalysts. *Polymer* **2017**, *131*, 151–159. (c) Yu, X.; Li, M.; Hong, J.; Zhou, X.; Zhang, L. Living 3,4-(Co)Polymerization of Isoprene/Myrcene and One-Pot Synthesis of a Polyisoprene Blend Catalyzed by Binuclear Rare-Earth Metal Amidinate Complexes. *Eur. J.* **2019**, *25*, 2569–2576.
- (12) Kim, B.-S.; Jiménez, J.; Gao, F.; Walsh, P. J. Palladium-Catalyzed Benzylic C–H Arylation of Azaaryl methylamines. *Org. Lett.* **2015**, *17*, 5788–5791.
- (13) (a) Addison, A. W.; Rao, T. N.; Reedijk, J.; van Rijn, J.; Verschoor, G. C. Synthesis, Structure, and Spectroscopic Properties of Copper(II) Compounds containing Nitrogen-Sulphur Donor Ligands; the Crystal and Molecular Structure of Aqua[1,7-bis(N-methylbenzimidazol-2'-yl)-2,6-dithiaheptane]copper(II) Perchlorate. *J. Chem. Soc., Dalton Trans.* **1984**, 1349–1356. (b) Annunziata, L.; Pragliola, S.; Pappalardo, D.; Tedesco, C.; Pellecchia, C. New (Anilidomethyl)pyridine Titanium(IV) and Zirconium(IV) Catalyst Precursors for the Highly Chemo- and Stereoselective 1,4-Polymerization of 1,3-Butadiene. *Macromolecules* **2011**, *44*, 1934–1941.
- (14) Zheng, T.; Liao, H.; Gao, J.; Zhong, L.; Gao, H.; Wu, Q. Synthesis and characterization of  $\alpha$ -diamine palladium complexes and insight into hybridization effects of nitrogen donor atoms on norbornene (co)polymerizations. *Polym. Chem.* **2018**, *9*, 3088–3097.
- (15) Wang, L.; Wang, X.; Hou, H.; Zhu, G.; Han, Z.; Yang, W.; Chen, X.; Wang, Q. An unsymmetrical binuclear iminopyridine-iron complex and its catalytic isoprene polymerization. *Chem. Commun.* **2020**, *56*, 8846–8849.
- (16) (a) Yao, C.; Liu, D.; Li, P.; Wu, C.; Li, S.; Liu, B.; Cui, D. Highly 3,4-Selective Living Polymerization of Isoprene and Copolymerization with  $\epsilon$ -Caprolactone by an Amidino N-Heterocyclic Carbene Ligated Lutetium Bis(alkyl) Complex. *Organometallics* **2014**, *33*, 684–691. (b) Yao, C.; Liu, N.; Long, S.; Wu, C.; Cui, D. Highly cis-1,4-selective coordination polymerization of polar 2-(4-methoxyphenyl)-1,3-butadiene and copolymerization with isoprene using a  $\beta$ -diketiminato yttrium bis(alkyl) complex. *Polym. Chem.* **2016**, *7*, 1264–1270.
- (17) Ricci, G.; Leone, G.; Boglia, A.; Boccia, A. C.; Zetta, L. cis-1,4-alt-3,4 Polyisoprene: Synthesis and Characterization. *Macromolecules* **2009**, *42*, 9263–9267.
- (18) Wang, X.-B.; Zhang, M.; Luo, L.; Hussain, M.; Luo, Y. A Computational Study of Isoprene Polymerization Catalyzed by Iminopyridine-Supported Iron Complexes: Ligand-Controlled Selectivity. *Chem. Phys. Lett.* **2020**, *755*, 137811.
- (19) Wang, B.; Bi, J.; Zhang, C.; Dai, Q.; Bai, C.; Zhang, X.; Hu, Y.; Jiang, L. Highly active and trans-1,4 specific polymerization of 1,3-butadiene catalyzed by 2-pyrazolyl substituted 1,10-phenanthroline ligated iron (II) complexes. *Polymer* **2013**, *54*, 5174–5181.
- (20) (a) Guo, L. H.; Lian, K. B.; Kong, W. Y.; Xu, S.; Jiang, G. R.; Dai, S. Y. Synthesis of Various Branched Ultra-High-Molecular-Weight Polyethylenes Using Sterically Hindered Acenaphthene-Based  $\alpha$ -Diimine Ni(II) Catalysts. *Organometallics* **2018**, *37*, 2442–2449. (b) Brown, L. A.; Anderson, W. C.; Mitchell, N. E.; Gmernicki, K. R.; Long, B. K. High Temperature, Living Polymerization of Ethylene by a Sterically-Demanding Nickel(II)  $\alpha$ -Diimine Catalyst. *Polymers* **2018**, *10*, 41–49.
- (21) Guo, J. J.; Zhang, W. J.; Oleynik, I. I.; Solan, G. A.; Oleynik, I. V.; Liang, T. L.; Sun, W. H. Probing the Effect of Ortho-cycloalkyl Ring Size on Activity and Thermostability in Cycloheptyl-fused N,N,N-iron Ethylene Polymerization Catalysts. *Dalton Trans.* **2020**, *49*, 136–146.
- (22) (a) Mahmood, Q.; Guo, J.; Zhang, W.; Ma, Y.; Liang, T.; Sun, W.-H. Concurrently Improving the Thermal Stability and Activity of Ferrous Precatalysts for the Production of Saturated/Unsaturated Polyethylene. *Organometallics* **2018**, *37*, 957–970. (b) Mahmood, Q.; Yue, E.; Guo, J.; Zhang, W.; Ma, Y.; Hao, X.; Sun, W.-H. Nitro-functionalized Bis(imino)pyridylferrous Chlorides as Thermo-stable Precatalysts for Linear Polyethylenes with High Molecular Weights. *Polymer* **2018**, *159*, 124–137.
- (23) Guo, J.; Wang, B.; Bi, J.; Zhang, C.; Zhang, H.; Bai, C.; Hu, Y.; Zhang, X. Synthesis, characterization and 1,3-butadiene polymerization studies of cobalt dichloride complexes bearing pyridine bisoxazoline ligands. *Polymer* **2015**, *59*, 124–132.